

Review

Review of the $\text{Yb}^{3+}:\text{ScBO}_3$ Laser Crystal Growth, Characterization, and Laser Applications

Dazhi Lu , Xiaoheng Li, Haohai Yu *, Huaijin Zhang * and Jiyang Wang

State Key Laboratory of Crystal Materials and Institute of Crystal Materials, Shandong University, Jinan 250100, China; dazhi.lu@sdu.edu.cn (D.L.); 202012868@mail.sdu.edu.cn (X.L.); jywang@sdu.edu.cn (J.W.)
* Correspondence: haohaiyu@sdu.edu.cn (H.Y.); huaijinzhang@sdu.edu.cn (H.Z.)

Abstract: Passive Q-switching is an effective approach for generating pulsed lasers, owing to its compact and additional modulation-free design. However, to compare favorably with active Q-switching and multi-stage amplification, the output energy needs to be enhanced for practical applications. Kramers Ytterbium ion (Yb^{3+})-doped borate crystals, with their excellent energy storage capacity, have been proven to be high-potential laser gain mediums for achieving pulsed lasers with moderate and high output energy using passive Q-switching technology. In this study, the growth, characterization, and laser generation of one Yb^{3+} -doped borate crystal, the $\text{Yb}^{3+}:\text{ScBO}_3$ crystal, are systematically reviewed. The continuous-wave and passive Q-switching laser characteristics are presented in detail, and the self-pulsations derived from intrinsic ground-state reabsorption are also demonstrated. The specific characteristics and experiments confirm the potential of the $\text{Yb}^{3+}:\text{ScBO}_3$ crystal for future pulsed laser applications with moderate or even high energy output.

Keywords: ytterbium-doped laser crystal; Czochralski crystal growth; solid-state lasers; passive Q-switching



Citation: Lu, D.; Li, X.; Yu, H.; Zhang, H.; Wang, J. Review of the $\text{Yb}^{3+}:\text{ScBO}_3$ Laser Crystal Growth, Characterization, and Laser Applications. *Appl. Sci.* **2021**, *11*, 10879. <https://doi.org/10.3390/app112210879>

Academic Editor: Yung-Fu Chen

Received: 28 October 2021
Accepted: 14 November 2021
Published: 17 November 2021

Publisher's Note: MDPI stays neutral with regard to jurisdictional claims in published maps and institutional affiliations.



Copyright: © 2021 by the authors. Licensee MDPI, Basel, Switzerland. This article is an open access article distributed under the terms and conditions of the Creative Commons Attribution (CC BY) license (<https://creativecommons.org/licenses/by/4.0/>).

1. Introduction

Pulsed lasers with typical single-pulse energy at the microjoule scale play vital roles in ranging, remote sensing, micro-machining, medical treatment, and other applications [1–6]. Generally, the commonly used passive Q-switching technology has been of great interest because it has a compact structure and no need for additional modulation and control systems, compared with active Q-switching technology, multi-stage amplification, etc. [7–12]. However, the output energy of passive Q-switching still needs to be improved to allow its use in practical applications. Based on the solid-state laser theory and the passive Q-switching rate equation, a laser gain medium with a high energy storage capacity is beneficial for moderate- and high-energy pulsed laser output [13,14]. Such a laser gain medium possesses desirable emission characteristics, such as a long fluorescence lifetime, small emission cross-section, and broad fluorescence spectra. The laser crystal, an important component of various laser gain media, is composed of doping ions and host materials. The comprehensive emission equities of the crystal are ascertained by the electronic structure and crystal field [15,16]. Therefore, laser crystals with favorable doping ions and host materials are desired for passive Q-switching laser applications.

Ytterbium ions (Yb^{3+}) with only two 4f electronic states have received considerable scrutiny due to its plentiful superior qualities, including concentration quenching, eradicated up-conversion, and excited-state absorption [16]. Meanwhile, they belong to the Kramers ions with uneven electrons in the 4f shell, which generate spin-orbit interactions among the electrons, as well as strong coupling between electrons and the crystal field [15,17]. Thus, Yb^{3+} -doped laser crystals generally possess relatively wide fluorescence spectra and long fluorescence lifetimes, which are conducive to moderate, and even high-energy, pulsed laser output. Many prominent Yb^{3+} -doped laser crystals have been developed, including the garnets (e.g., $\text{Yb}^{3+}:\text{Y}_3\text{Al}_5\text{O}_{12}$ (YAG) [18], $\text{Yb}^{3+}:\text{Y}_3\text{Ga}_5\text{O}_{12}$ (YGG) [19],

$\text{Yb}^{3+}:\text{Gd}_3\text{Ga}_5\text{O}_{12}$ (GGG) [20], $(\text{Yb}_x\text{Y}_{1-x})_3(\text{Sc}_{1.5}\text{Ga}_{0.5})\text{Ga}_3\text{O}_{12}$ (YSGG) [21], $\text{Yb}^{3+}:\text{Lu}_3\text{Ga}_5\text{O}_{12}$ (LuGG) [22]), tungstates (e.g., $\text{Yb}^{3+}:\text{KGd}(\text{WO}_4)_2$ (KGW) [23,24], $\text{Yb}^{3+}:\text{NaY}(\text{WO}_4)_2$ (NaYW) [25], $\text{Yb}^{3+}:\text{NaGd}(\text{WO}_4)_2$ (NaGdW) [26], $\text{Yb}^{3+}:\text{KLu}(\text{WO}_4)_2$ (KLuW) [27]), and borates ($\text{Yb}^{3+}:\text{YCa}_4\text{O}(\text{BO}_3)_3$ (YCOB) [28–30], $\text{Yb}^{3+}:\text{GdCa}_4\text{O}(\text{BO}_3)_3$ (GdCOB) [28,31]). Among them, Yb^{3+} -doped borates with short bond lengths (e.g., $\text{Yb}:\text{YCOB}$ and $\text{Yb}:\text{GdCOB}$) have relatively smaller emission cross-sections ($\sim 0.5 \times 10^{-20} \text{ cm}^2$), longer fluorescence lifetimes ($\sim 2 \text{ ms}$), broader emission spectra (45 nm), and have been proven to be excellent energy storage materials. For example, a passive Q-switching laser with a pulse energy of 1.02 mJ was achieved in 2016, using GaAs as the saturable absorber [29].

In 1993, the spectral characteristics of $\text{Yb}^{3+}:\text{ScBO}_3$ crystal were reported, with an emission cross-section of $\sim 0.1 \times 10^{-20} \text{ cm}^2$ and a fluorescence lifetime of $\sim 5 \text{ ms}$, indicating that it can be an ideal gain medium for obtaining Q-switching lasers with moderate or high pulse energy [32]. However, the growth difficulties of $\text{Yb}^{3+}:\text{ScBO}_3$ crystal with its high optical quality have hindered further progress in laser applications. Most recently, the first optical grade $\text{Yb}^{3+}:\text{ScBO}_3$ crystal was successfully grown and both CW and passive Q-switching lasers have been realized [33,34]. In addition, the growth method, characteristics, and laser performance of $\text{Yb}^{3+}:\text{ScBO}_3$ crystal has been systematically reviewed. The self-Q-switching characteristics derived from intrinsic ground-state reabsorption are also discussed. All results presented a high potential gain medium for moderate- or even high-energy pulsed laser generation using both active and passive Q-switching technologies.

2. Bulk Crystal Characteristics

2.1. Crystal Structure

The ScBO_3 crystal remains a trigonal crystal system, a $\bar{3}m1$ point group, and a $R\bar{3}c$ space group. As exhibited in Figure 1a, the Sc atoms and O atoms are coordinated to form ScO_6 octahedra, which are connected to each other to form a pore structure. The B atoms are located in the pores and coordinate with the O atoms to form BO_3 tetrahedra. In addition, the effective ionic radii of Yb^{3+} and Sc^{3+} are 0.868 and 0.745 Å [35], respectively, which is beneficial, even for the Yb^{3+} -dropped and lattice pattern distortion in $\text{Yb}^{3+}:\text{ScBO}_3$ crystals.

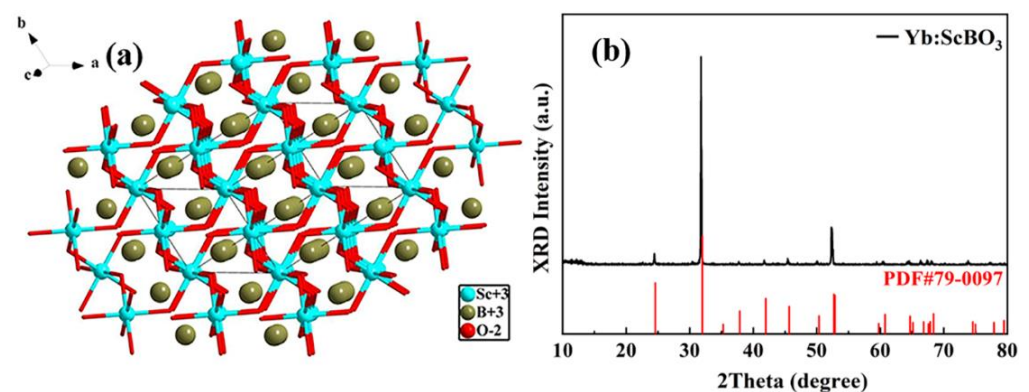
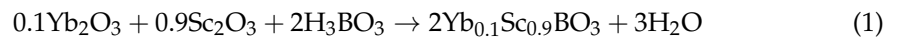


Figure 1. (a) Structural diagram of ScBO_3 and (b) comparison between X-ray powder diffraction pattern of standard PDF#79-0097 and $\text{Yb}^{3+}:\text{ScBO}_3$ crystal [34].

The diffraction indices of ScBO_3 crystal, measured by X-ray powder diffraction, matched well with standard PDF#79-0097, as exhibited in Figure 1b. After calculations, the cell parameters of ScBO_3 were obtained: $a = b = 4.776 \text{ \AA}$ and $c = 15.405 \text{ \AA}$. When doped with the Yb^{3+} ion, the cell parameters and crystal structure apparently do not adjust compared with undoped ScBO_3 crystal [36]. Here, the buoyancy method was applied for measuring crystal density, and the result was 3.787 g/cm^3 , which corresponded with the theoretical density of 3.812 g/cm^3 .

2.2. Crystal Growth

ScBO₃ crystals are usually grown utilizing the Czochralski method due to the congruent characteristics of this crystal [37]. However, difficulties, such as the intense volatilization of B₂O₃, not only lead to segregation of the composition, but also give rise to instability in growth, which greatly affects the optical quality of the crystals [37]. Here, a 10.0 at.% Yb³⁺-doped ScBO₃ single crystal with a 20-mm-diameter was successfully grown using an argon atmosphere in an iridium crucible. The starting materials, Yb₂O₃, Sc₂O₃, and H₃BO₃, were weighed according to the chemical formula Yb_{0.1}Sc_{0.9}BO₃. Generally, an additional 3wt% H₃BO₃ was put in the raw ingredients during the batching process, which was used to compensate for B₂O₃ volatilization during crystal growth and polycrystalline material preparation. The equation for the chemical reaction is as follows:



A mullite brick with an appropriate thickness was used in the furnace to create a large temperature gradient to avoid constitutional supercooling and reduce volatilization. First, the seed was a platinum wire to obtain polycrystal with plenty of cracks, as shown in Figure 2a. To diminish the cracking, the seed was cut from the bulk polycrystal along *c*-axis. Meanwhile, a micro-convex solid–liquid interface was achieved by optimizing the temperature field and rotation speed, thereby balancing the natural convection and forced convection during the growth process. Although some subsidiary white matter took shape owing to the volatilization, the samples for laser experiments (as presented in the inset of Figure 2b) could be extracted from this optical-quality crystal (Figure 2b). Polycrystalline material was used as the standard to measure and calculate the density of elemental Yb³⁺ in this crystal. The effective distribution coefficient of Yb³⁺ was ascertained as 0.95.

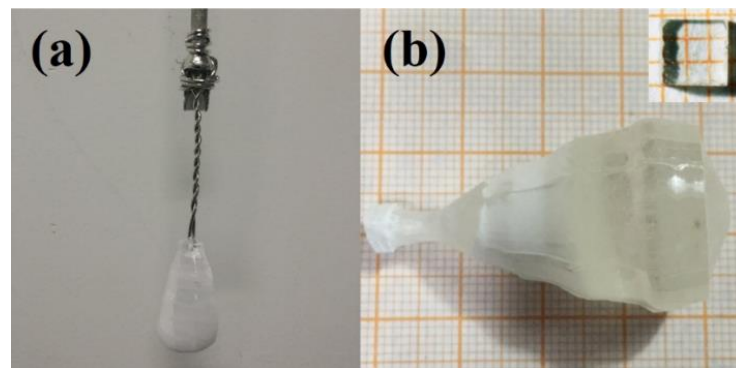


Figure 2. (a) Yb³⁺:ScBO₃ crystal grown with a seed of platinum wire, (b) optical-quality Yb³⁺:ScBO₃ crystal. Inset: cut and polished laser sample. (Source: [34], © 2015 Optica Publishing Group, Washington, DC, USA).

2.3. Thermal Characteristics, Laser Damage Threshold and Mechanical Characteristics

Laser performance and crystal growth are usually affected by thermal expansion, specific heat, and so on [38]. Laser crystals are liable to break during the growth process, usually owing to obvious anisotropic thermal expansion, low thermal conductivity, and low specific heat. Meanwhile, the crystal may have a significant thermal effect during the laser experiment process due to a large temperature gradient.

The specific heat capacity was measured and then calculated using a thermal analyzer and software produced by Perkin-Elmer Co., Waltham, MA, USA. The specific heat (*C_p*) of Yb³⁺:ScBO₃ increased with temperature, and the median was 0.73 J·g^{−1}·K^{−1} at 330 K, as shown in Figure 3a [36,39]. Because of a large specific heat, compared with Yb³⁺:YCOB (0.75 J·g^{−1}·K^{−1}) and Yb³⁺:YVO₄ (0.62 J·g^{−1}·K^{−1}), Yb³⁺:ScBO₃ will not be extremely influenced by the heat caused during the laser emission action and a very large damage threshold can be forecast.

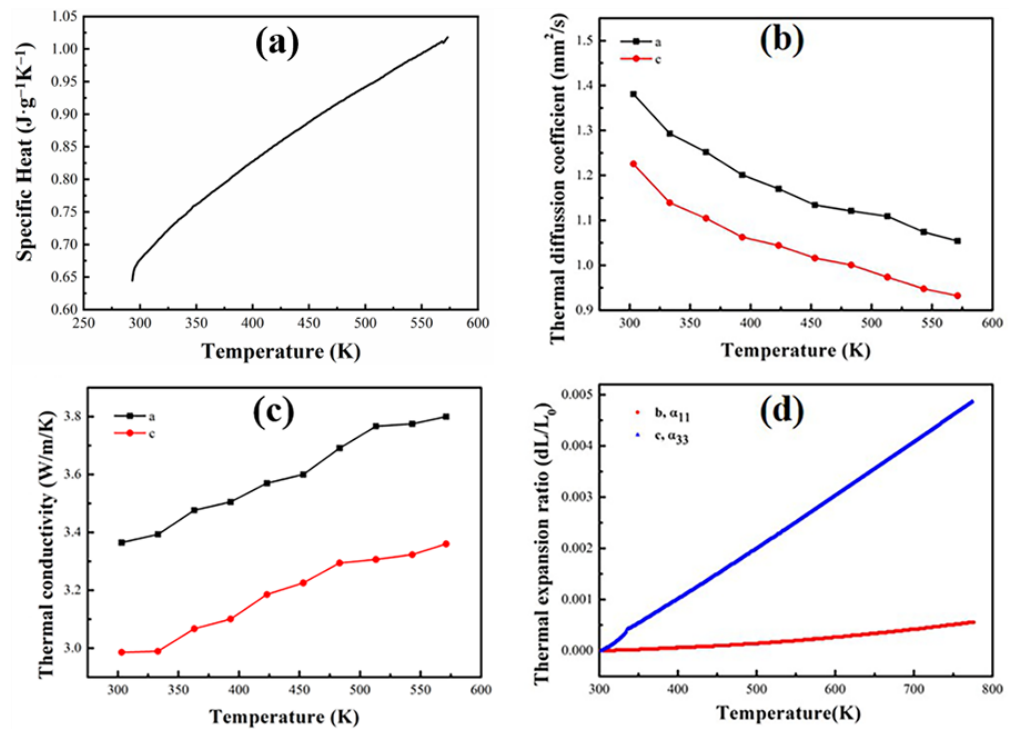


Figure 3. Thermal characteristics of $\text{Yb}^{3+}:\text{ScBO}_3$ as a function of temperature: (a) specific heat, (b) thermal diffusion coefficient, (c) thermal conductivity with temperature, and (d) thermal expansion coefficient [34].

A laser flash apparatus was used to take stock of the thermal diffusivity; the findings are shown in Figure 3b, which shows a plot of the thermal diffusivity (λ_{ij}) of $\text{Yb}^{3+}:\text{ScBO}_3$ at temperatures ranging from 303.15 K to 774.15 K.

In view of the following equation, the thermal conductivity (k) was determined:

$$k = \lambda_{ij} \rho C_p \quad (2)$$

when the temperature increased at above temperatures range, the a -axis thermal conductivity increased from $3.61 \text{ W}\cdot\text{m}^{-1}\cdot\text{K}^{-1}$ to $3.86 \text{ W}\cdot\text{m}^{-1}\cdot\text{K}^{-1}$, and the c -axis thermal conductivity also increased from $2.98 \text{ W}\cdot\text{m}^{-1}\cdot\text{K}^{-1}$ to $3.36 \text{ W}\cdot\text{m}^{-1}\cdot\text{K}^{-1}$ (as presented in Figure 3c). Owing to the tendency of the thermal conductivity to rise with rising temperature, this crystal can be utilized in generating medium lasers.

The α_{ij} of one crystal, which is a meristic second-order tensor, represents the thermal expansion coefficient [40]. Since $\text{Yb}^{3+}:\text{ScBO}_3$ appertain a trigonal system, on account of the principle of Neumann, the thermal expansion coefficient tensor is exhibited to be:

$$\begin{pmatrix} \alpha_{11} & 0 & 0 \\ 0 & \alpha_{22} & 0 \\ 0 & 0 & \alpha_{33} \end{pmatrix} \quad (3)$$

According to the crystal structure, $\text{Yb}^{3+}:\text{ScBO}_3$ has two thermal expansion coefficients, α_{11} and α_{33} , which are independent. The measurements of the thermal expansion tensor of this crystal were utilized a thermal mechanical analyzer (Diamond TMA). Moreover, the thermal expansion curves of $\text{Yb}^{3+}:\text{ScBO}_3$, plotted versus temperature, are presented in Figure 3d. The two aforementioned thermal expansions remained virtually linear. Then, the thermal expansion coefficients along these two axes were separately determined to be $1.05 \times 10^{-6} \text{ K}^{-1}$ for α_{11} and $10.24 \times 10^{-6} \text{ K}^{-1}$ for α_{33} . The considerable anisotropy in terms

of thermal expansion may lead to cracking during the crystal growth process. The density at diverse temperatures for $\text{Yb}^{3+}:\text{ScBO}_3$ was determined utilizing the following formula:

$$\rho = \frac{m}{abc} = \frac{m}{a_0 b_0 c_0} \frac{1}{\left(1 + \frac{\Delta a}{a_0}\right) \left(1 + \frac{\Delta b}{b_0}\right) \left(1 + \frac{\Delta c}{c_0}\right)} = \frac{\rho_0}{\left(1 + \frac{\Delta a}{a_0}\right) \left(1 + \frac{\Delta b}{b_0}\right) \left(1 + \frac{\Delta c}{c_0}\right)} \quad (4)$$

where theoretical density ρ_0 is 3.812 g/cm^3 . The data were fitted to a linear formula, as shown in the result: $\rho = (-5 \times 10^{-5})T + 3.83$.

To measure the laser damage threshold, a Q-switched pulsed laser with an emission wavelength of 1064 nm was utilized. Then, the damage threshold of the $\text{Yb}^{3+}:\text{ScBO}_3$ crystal was 509 MW/cm^2 . The threshold value of $\text{Yb}^{3+}:\text{ScBO}_3$ was almost half that of $\text{Yb}^{3+}:\text{YVO}_4$ and $\text{Yb}^{3+}:\text{YAG}$.

For the purpose of acquiring the hardness of the sample, a digital microhardness tester was utilized. The hardness was determined using the following equation:

$$H_v = 1.8544 P/d^2 \quad (5)$$

where H_v is the Vickers hardness, d is trace length along the diagonal, and P is the load. The Vickers hardness of the as-grown crystal along the a , b , and c axes was tested to be 7.05, 6.85, and 10.67 GPa, respectively. The hardness along the a and b axes was anisotropic with comparable values. The $\text{Yb}^{3+}:\text{ScBO}_3$ crystal had modest hardness, which was smaller than that of YAG (12.7 GPa) [41] and bigger than that of YVO_4 (4.8 GPa) [42]. Thus, the $\text{Yb}^{3+}:\text{ScBO}_3$ crystal may be incised efficiently.

2.4. Spectroscopic Characteristics

A spectrophotometer, with a spectral sharpness of separation of 0.2 nm, was used to determine the room temperature (RT) absorption spectra. The cutting orientation of the sample was along the a axis. An Edinburgh Instruments FLS920 fluorescence spectrometer was utilized to determine both the room and cryogenic (79 K) fluorescence properties, and the thickness of the sample was 0.5 mm. The absorption spectra and RT fluorescence of $\text{Yb}^{3+}:\text{ScBO}_3$ are presented in Figure 4a. The main absorption peak was at 964.8 nm. Its full-width at half maximal (FWHM) was determined to be 19.86 nm, and the absorption cross-section was determined to be $0.13 \times 10^{-20} \text{ cm}^2$. Diode laser sources are appropriate for the wide absorption bandwidth. At 79 K, the zero-photon line was at 964 nm, as exhibited in Figure 4a. Figure 4b exhibits the energy levels of the Yb^{3+} ions in the ScBO_3 crystal [43].

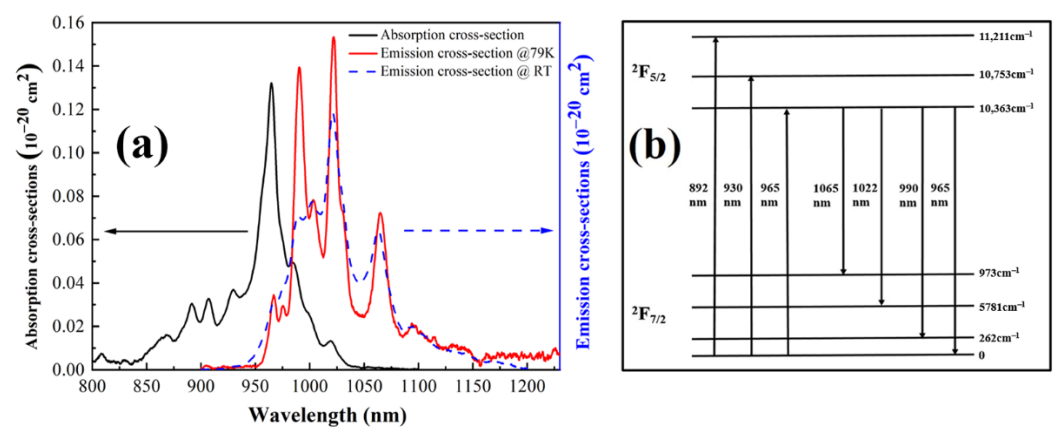


Figure 4. (a) Emission cross-section spectra (RT and 79K) and absorption cross-section (RT) spectra; (b) diagram of energy level. (Source: [34], © 2015 Optica Publishing Group, Washington, DC, USA).

The cross-section of the RT emission was determined using the following formula [32,44]:

$$\sigma_{em}(\lambda) = \frac{\lambda^4 I(\lambda)}{8\pi c n^2 \tau_{rad} \int I(\lambda) d\lambda} \quad (6)$$

where $I(\lambda)$ represents the emission intensity, n represents the refractive index, and τ_{rad} represents the radiative lifetime. As exhibited in Figure 4a, the strongest emission peak (λ_{peak}) was at 1021 nm. Meanwhile, the corresponding emission cross-section (σ_{em}) was determined to be $0.12 \times 10^{-20} \text{ cm}^2$, which was significantly larger than that of $\text{Yb}^{3+}:\text{YAG}$ [45] and $\text{Yb}^{3+}:\text{YGG}$ [46,47].

After testing and fitting, it was determined that the fluorescence lifetime at room temperature was 5.25 ms [48], as shown in Figure 5. Both the exponential and linear fitted decay curves provided the single exponential trend, as shown in Figure 5 [49]. Table S1 lists the passive Q-switching performance and corresponding spectral and thermal characteristics of commonly used Yb^{3+} -doped crystals, such as $\text{Yb}^{3+}:\text{YAG}$, $\text{Yb}^{3+}:\text{YGG}$, $\text{Yb}^{3+}:\text{KGW}$, $\text{Yb}^{3+}:\text{YCOB}$, and $\text{Yb}^{3+}:\text{GdCOB}$. Among them, the $\text{Yb}^{3+}:\text{ScBO}_3$ crystal possesses the smallest emission cross-section, the longest fluorescence lifetime, and a moderate fluorescence linewidth, indicating its excellent potential for achieving pulsed lasers with moderate, or even high, pulse energy.

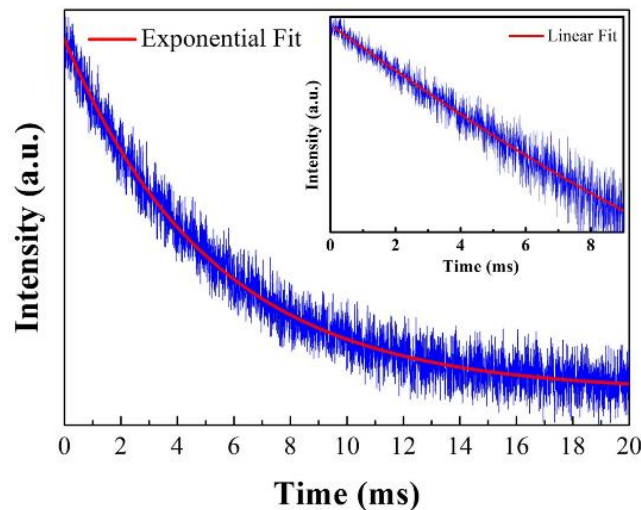


Figure 5. RT fluorescence lifetime fitted by exponential functions. Inset: the linear fitted lifetime with log (intensity) vs. time. (Source: [34], © 2015 Optica Publishing Group, Washington, DC, USA).

2.5. Continuous Laser Performance

The effective gain cross-section (σ_g) of $\text{Yb}^{3+}:\text{ScBO}_3$ was determined using the following formula before the lasing experiments, as presented in Figure 6:

$$\sigma_g(\lambda) = \beta\sigma_{em}(\lambda) - (1 - \beta)\sigma_{abs}(\lambda) \quad (7)$$

where β is the proportion of the active ions excited to the upper level. The least value of $\beta_{min}(1021 \text{ nm})$ is determined using the following formula:

$$\beta_{min}(1021 \text{ nm}) = \frac{\sigma_{abs}(1021 \text{ nm})}{\sigma_{abs}(1021 \text{ nm}) + \sigma_{em}(1021 \text{ nm})} = 0.1 \quad (8)$$

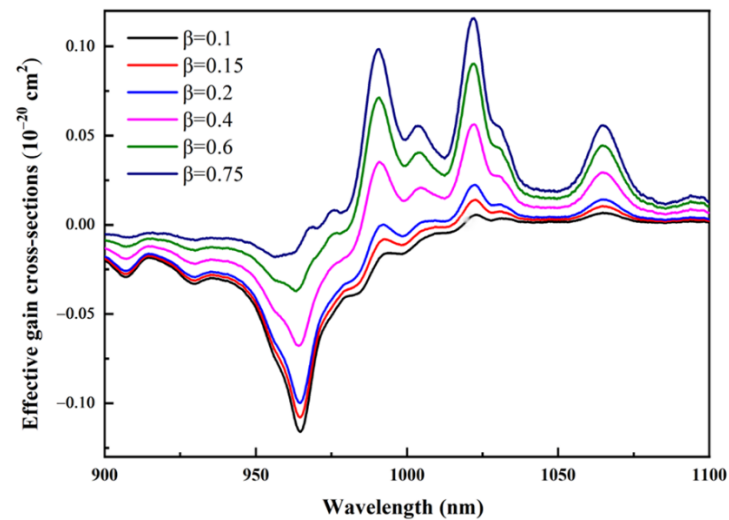


Figure 6. $\sigma_g(\lambda)$ of $\text{Yb}^{3+}:\text{ScBO}_3$ crystal versus wavelength. (Source: [34], © 2015 Optica Publishing Group, Washington, DC, USA).

The positive part of σ_g is presented in Figure 6 as different values of β . When $\beta = 0.75$, the positive extent, which resembles $\text{Yb}^{3+}:\text{YAG}$ (950–1080 nm) [50], $\text{Yb}^{3+}:\text{CYB}$ (960–1100 nm), and $\text{Yb}^{3+}:\text{CaGB}$ (960–1100 nm), was 970–1100 nm [47,51]. The excellent characteristics of these crystal are suitable for tunable and femtosecond lasers. When $\beta = 0.75$, $\text{Yb}^{3+}:\text{ScBO}_3$ could, in theory, back a pulse continuation of 65 fs. The correlation between the gain bandwidth ($\Delta\nu$) and the shortest pulse duration (t_{FWHM}) was used to determine the pulse continuation [52]:

$$t_{FWHM} \cdot \Delta\nu = 0.315 \quad (9)$$

The experimental configuration is depicted in Figure 7 and a plane–concave cavity, which was 42 mm in length, was applied for CW laser generation. The emission wavelength of the pump source was 976 nm and the crystal was cut along the a axis, uncoated, and burnished. Furthermore, the input coupler had a high reflectance, from 1000 to 1100 nm, and a transmittance of over 99.5% at 950–990 nm. The transmittance from 1000–1100 nm of the output coupler was 5%.

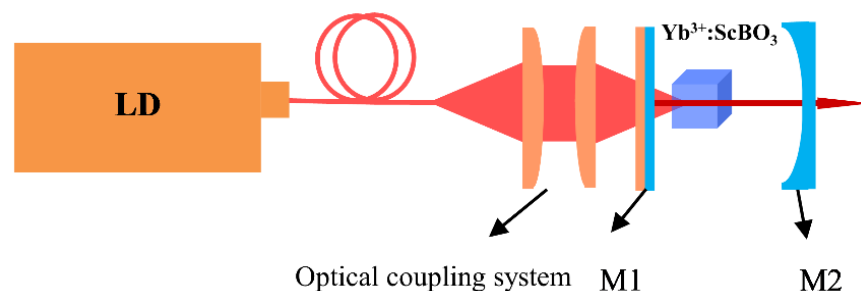


Figure 7. The experimental setup of continuous laser. (Source: [34], © 2015 Optica Publishing Group, Washington, DC, USA).

A CW laser has been demonstrated and the corresponding laser performance is exhibited in Figure 8. It indicates that the threshold was 2.38 W. Under a 4.9-W pump power, the output power rose to 167 mW, and the slope efficiency was 9% at a wavelength of 1.063 μm . The light-to-light conversion efficiencies, calculated from the data above, are 4% and 9%, respectively. The laser performance can be greatly enhanced by utilizing a higher transmission of the output couplers, mode matching, coating conditions, etc.

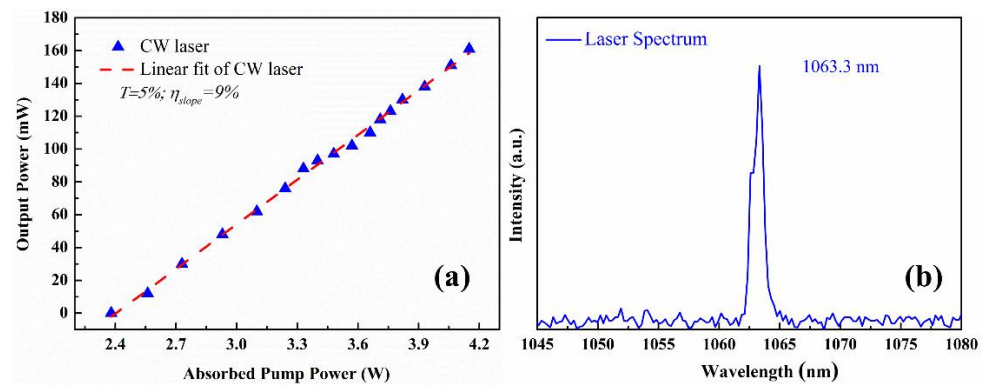


Figure 8. (a) Pump power versus average output power and (b) laser spectra [33].

2.6. Q-Switching Laser Performance

As mentioned earlier, the Yb^{3+} -doped ScBO_3 crystal has an excellent energy storage capacity, which is favorable for Q-switching pulse generation with moderate or even high output energy. Meanwhile, the passive Q-switching properties were characterized when utilizing the polished and uncoated $\text{Yb}^{3+}:\text{ScBO}_3$ laser crystal and black phosphorous (BP) as the saturable absorber [33]. This crystal sample was incised along the a axis and enclosed in a water-cooled Cu block at 2°C . A plane-concave cavity was applied, which was the same as that of the CW laser configuration described earlier.

The CW laser could be discovered without the BP optical switcher, as shown in Figure 8. When BP was inserted into the cavity, the pulsed laser was generated with the threshold of 3.3 W, the slope efficiency of 5%, and the highest average output power was 43 mW, as illustrated in Figure 9a. The obvious threshold diversity between the pulsed lasers and CW was observed by means of the small emission cross-section of the crystal. In the meantime, the threshold was increased owing to the reflection loss, which was attributed to the coating-less wafer.

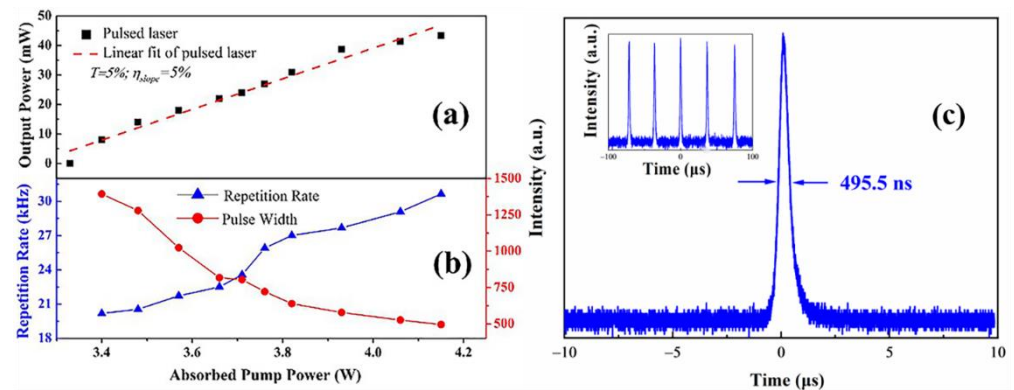


Figure 9. (a) Pump power versus average pulsed output power, (b) pump power as a function of repetition frequency and pulse width, respectively, and (c) single pulse. Inset: pulsed train [33].

The pump power versus the repetition frequency and pulse width are shown in Figure 9b. Under a pump power of 3.4 W, the pulse width was 1393 ns and the repetition frequency was 20 kHz. When the absorption pump power was 4.15 W, the pulse width was 495.5 ns, and the repetition frequency was 30.6 kHz. With the increasing power of the pump, the trends of the pulse width and repetition frequency were opposite. The above phenomenon is a characteristic of passive Q-switching lasers [53,54]. Under an average output power of 43 mW, the maximal pulse energy was $1.4 \mu\text{J}$, which was notably higher than the acquired pulse energy in the BP-modulated $\text{Yb}^{3+}:\text{CYA}$ crystal. The energy storage capacity was also notably better than that of $\text{Yb}^{3+}:\text{CYA}$ [55,56], because of the smaller emission cross-section and longer fluorescence lifetime. The inset of Figure 9c shows a

characteristic pulsed train with a repetition frequency of 29 kHz. The narrowest pulse width was determined to be 495.5 ns, as shown in Figure 9c. The beam size for the BP sample was determined to be 181.9 μm , based on the ABCD matrix [57]. In the meantime, the beam properties, with a size of 225.5 μm and a M^2 factor of 1.2, were evaluated using a CCD (CinCam COMS-1201). Therefore, stable passive Q-switching was achieved, indicating that moderate- and high-energy pulses can be achieved in this gain medium, under both active and passive Q-switching regimes.

Moreover, self-Q-switching operation was also demonstrated in $\text{Yb}^{3+}:\text{ScBO}_3$ crystal under the same diode pump configuration, but with a plane–plane cavity configuration. Here, a laser sample with dimensions of $2 \times 3 \times 3 \text{ mm}^3$ and the output couplers with transmittances of 1% and 3% were utilized. Figure 10 shows the relevant characteristics of the output beam, including the output power versus the absorbed pump power (Figure 10a), the laser spectra (Figure 10b), and the beam profile (inset of Figure 10b). As the transmittance of the output coupler increased from 1% to 3%, the threshold of the absorption pump power increased from 0.81 W to 1.26 W, the maximal output power increased from 312 mW to 332 mW, and the corresponding slope efficiency increased from 27.9% to 39.8%. The slope efficiency and output power were improved compared with the study on the Q-switching process modulated by BP [33], because both the laser crystal and cavity design were optimized. The laser spectra of the output lasers are exhibited in Figure 10b. The center wavelength is 1063.9 nm and the laser profile was detected by CCD (CinCam COMS-1201), which is shown in the inset of Figure 10b and is close to the fundamental transverse electromagnetic mode (TEM₀₀).

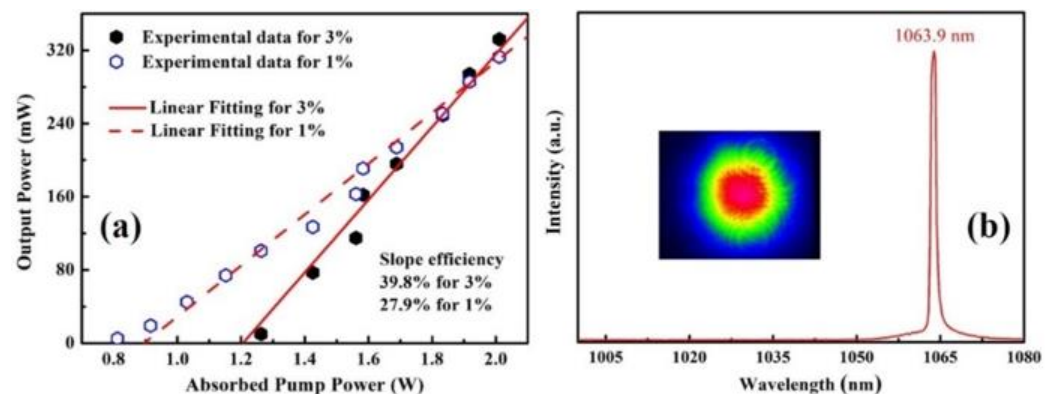


Figure 10. (a) Absorbed pump power versus average pulsed output power in the self-Q-switching operation (dots for the experimental data and lines for the linear fittings); (b) spectra and beam profile of the output laser.

As presented in Figure 11, the temporal characteristics of self-Q-switching pulses, which are the pump power versus the repetition frequency and pulse width, were determined with an oscillator combined with a silicon detector. Because the pump power improved from 0.81 to 2 W, the pulse width was shortened from 1674 to 541.8 ns; however, when using the 1% output coupler, the repetition frequency presented the opposite trend. In the meantime, the absorbed pump power improved from 1.26 to 2 W and the pulse width reduced from 1329 to 731.1 ns when using the transmittance of the 3% output coupler. Here, the repetition frequency also revealed the opposite trend. These trends are typical in passive Q-switching lasers [53,54].

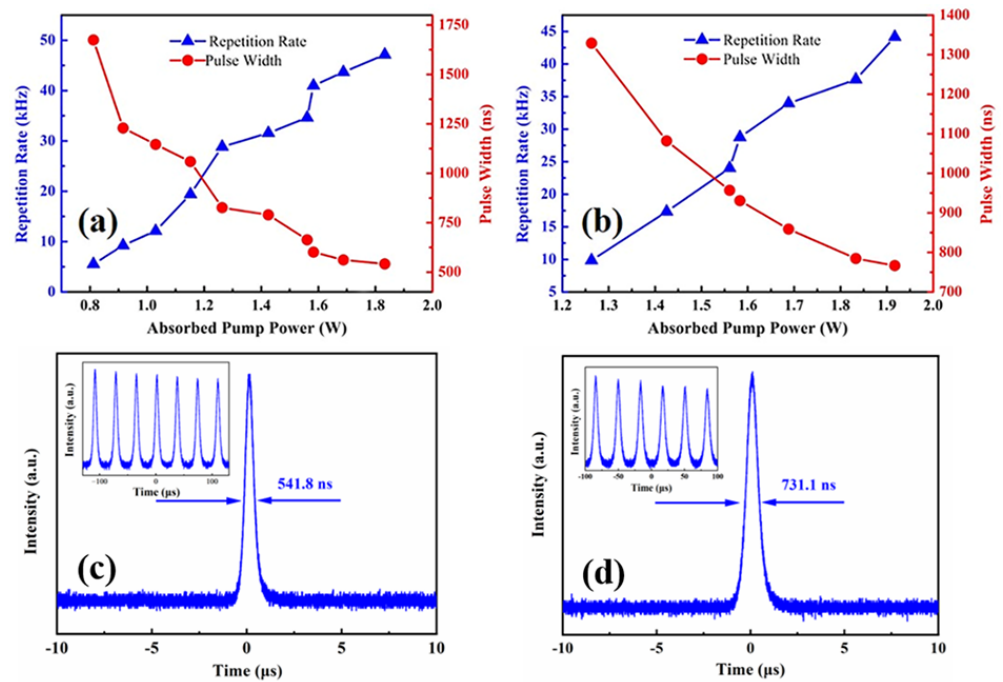


Figure 11. Absorption pump power versus repetition frequency and pulse width: (a) output coupler transmittance of 1%; (b) output coupler transmittance of 3%; (c) single pulse and pulse train with the output coupler transmittance of 1%; and (d) single pulse and pulse train with the output coupler transmittance of 3%.

As shown in Figure 11a,b, because the absorption pump power increased, the repetition frequency and the pulse width curves flattened. For the 1% and 3% output couplers, the shortest pulse widths were 541.8 ns and 731.1 ns, and the maximal repetition frequencies were 46.1 kHz and 38.8 kHz, respectively. The single pulses with minimum pulse widths, mentioned earlier, are shown in Figure 11c,d, and the relevant pulse trains are shown in the insets. The pulse energy can be calculated from the values of the output power and the repetition frequency. If combined with the pulse width, the peak power can also be obtained. When using the 1% output coupler, the maximal peak power was 9.8 W and the maximal pulse energy was determined to be 5.3 μJ . The maximal peak power was 10.2 W, and the maximal pulse energy was 7.3 μJ as using the 3% transmittance output coupler.

The nonlinear optical characteristics of the $\text{Yb}^{3+}:\text{ScBO}_3$ crystal were determined using a Z-scan test. Figure 12 shows the transmittance versus input energy intensity of the crystal when the $\text{Yb}^{3+}:\text{ScBO}_3$ crystal was at a wavelength of 1064 nm. The data were fitted utilizing the equation below [58]:

$$T = A \exp\left[\frac{-\delta\alpha}{1 + I/I_s}\right] \quad (10)$$

where A represents the normalized parameter, $\delta\alpha$ represents the saturable absorption, I represents the incident intensity, and I_s represents the saturation intensity. Furthermore, transmittance and intensity have a nonlinear relationship. Through fitting, the modulation depth of the $\text{Yb}^{3+}:\text{ScBO}_3$ sample was 17.77%. In addition, the absolute modulation depth was 10.2% and the saturation intensity was $4.1 \times 10^8 \text{ W/m}^2$ at 1064 nm.

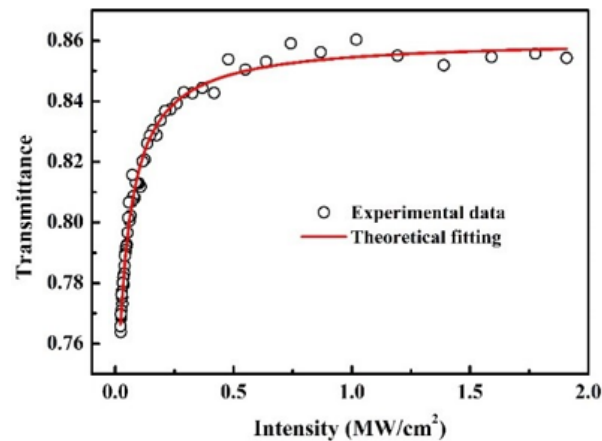


Figure 12. The transmittance versus input energy intensity of $\text{Yb}^{3+}:\text{ScBO}_3$ crystal.

As previously reported, the $\text{Yb}^{3+}:\text{ScBO}_3$ crystal was expected to have strong inversion population accumulation owing to its large excited-state lifetime and small emission cross-section [34]. Hence, the self-Q-switching process in the $\text{Yb}^{3+}:\text{ScBO}_3$ crystal can be attributed to the ground-state reabsorption, which is the saturable nature of the reabsorption loss at the lower level, $^2F_{7/2}$ [59–61]. All the results contribute to an understanding of the self-Q-switching in gain mediums with strong reabsorption effects, and aid in the development of the highly compact pulsed laser systems.

3. Conclusions

The growth, structure, physical characteristics, and laser performance of $\text{Yb}^{3+}:\text{ScBO}_3$ crystal with an excellent energy storage capacity are comprehensively reviewed, for both CW and passive Q-switching laser characteristics. After partially overcoming difficulties, such as the intense volatilization of B_2O_3 , a bulk crystal was triumphantly grown using the Czochralski technique. However, the optical quality is still required to be improved since there are lots of inclusions, as presented above, although the Czochralski method has been proved to be feasible. The thermal properties of the $\text{Yb}^{3+}:\text{ScBO}_3$ crystal, consisting of thermal conductivity and specific heat and so on, were characterized. In addition, the $\text{Yb}^{3+}:\text{ScBO}_3$ crystal was found to possess a small emission cross-section of $0.12 \times 10^{-20} \text{ cm}^2$ and a long fluorescence lifetime of 5.2 ms, which is beneficial for generating moderate and high-energy pulsed lasers. A CW laser, with a maximal output power of 167 mW and a slope efficiency of 9% under the wavelength of $1.063 \mu\text{m}$, was first obtained in the $\text{Yb}^{3+}:\text{ScBO}_3$ crystal, utilizing a plane–concave cavity configuration. Then, a passive Q-switching laser in this crystal was achieved utilizing BP as the optical modulator, with a minimum pulse width of 495.5 ns and a maximal pulse energy of 1.4 μJ . The consequences show the feasibility of $\text{Yb}^{3+}:\text{ScBO}_3$ crystal achieving pulsed lasers with moderate or high energy. Finally, the self-Q-switching and nonlinear optical characteristics of this crystal were evaluated and the mechanism was attributed to ground state re-absorption. The preferable spectroscopic characteristics and preliminary laser performances indicate that the as-grown $\text{Yb}^{3+}:\text{ScBO}_3$ crystal would be a high-potential laser gain medium in establishing compact pulsed laser systems with moderate or even high energy output. Future research will be dedicated to the optimization of the crystal growth in the aspects of establishing the thermal field with small gradient and searching for the optimal growth parameters, including pulling and rotation rates, etc. In the meantime, the actively Q-switched pulsed lasers with high energy output are also expected in the $\text{Yb}^{3+}:\text{ScBO}_3$ crystal.

Supplementary Materials: The following are available online at <https://www.mdpi.com/article/10.3390/app112210879/s1>, Table S1. Passively Q-switching performance and corresponding spectral and thermal properties in commonly used Yb^{3+} -doped crystals.

Author Contributions: Conceptualization, H.Y., H.Z. and J.W.; Data collection, X.L. and D.L.; writing—original draft preparation, X.L. and D.L.; writing—review and editing, D.L. and H.Y.; supervision, H.Y., H.Z. and J.W. All authors have read and agreed to the published version of the manuscript.

Funding: This work was supported by the National Natural Science Foundation of China (NSFC) (Grant 51902181) and Future Plans of Young Scholars at Shandong University.

Institutional Review Board Statement: Not applicable.

Informed Consent Statement: Not applicable.

Data Availability Statement: All the data reported in the paper are not publicly available at this time but maybe provided upon reasonable request.

Conflicts of Interest: The authors declare no competing financial interest.

References

1. Holzrichter, J.F.; Eimerl, D.; George, E.V.; Trenholme, J.B.; Simmons, W.W.; Hunt, J.T. High Power Pulsed Lasers. *J. Fusion Energy* **1982**, *2*, 5–45. [\[CrossRef\]](#)
2. Moskalik, K.; Kozlov, A.; Demin, E.; Boiko, E. The Efficacy of Facial Skin Cancer Treatment with High-Energy Pulsed Neodymium and Nd:YAG Lasers. *Photomed. Laser Surg.* **2009**, *27*, 345–349. [\[CrossRef\]](#) [\[PubMed\]](#)
3. Kumkar, M.; Bauer, L.; Russ, S.; Wendel, M.; Kleiner, J.; Grossmann, D.; Bergner, K.; Nolte, S. Comparison of Different Processes for Separation of Glass and Crystals Using Ultrashort Pulsed Lasers. *Proc. SPIE* **2014**, *8972*, 897214.
4. Maharjan, N.; Zhou, W.; Zhou, Y.; Guan, Y.; Wu, N. Comparative Study of Laser Surface Hardening of 50CrMo4 Steel Using Continuous-Wave Laser and Pulsed Lasers With Ms, ns, Ps and Fs Pulse Duration. *Surf. Coat. Technol.* **2019**, *366*, 311–320. [\[CrossRef\]](#)
5. McKenzie, R.L. Measurement Capabilities of Planar Doppler Velocimetry Using Pulsed Lasers. *Appl. Opt.* **1996**, *35*, 948–964. [\[CrossRef\]](#)
6. Baac, H.W.; Uribe-Patarroyo, N.; Bouma, B.E. High-Energy Pulsed Raman Fiber Laser for Biological Tissue Coagulation. *Opt. Express* **2014**, *22*, 7113–7123. [\[CrossRef\]](#) [\[PubMed\]](#)
7. Dergachev, A.; Armstrong, D.; Smith, A.; Drake, T.; Dubois, M. 3.4- μm ZGP RISTRA Nanosecond Optical Parametric Oscillator Pumped by a 2.05- μm Ho:YLF MOPA System. *Opt. Express* **2007**, *15*, 14404–14413. [\[CrossRef\]](#)
8. Axenson, T.J.; Barnes, N.P.; Reichle, D.J.; Koehler, E.E. High-Energy Q-Switching 0.946- μm Solid-State Diode Pumped Laser. *J. Opt. Soc. Am. B* **2002**, *19*, 1535–1538. [\[CrossRef\]](#)
9. Zhang, X.; Zhao, S.; Wang, Q.; Ozygus, B.; Weber, H. Modeling of Passive Q-Switching Lasers. *J. Opt. Soc. Am. B* **2000**, *17*, 1166–1175. [\[CrossRef\]](#)
10. Zayhowski, J.J. Passive Q-Switching Nd:YAG Microchip Lasers and Applications. *J. Alloy. Compd.* **2000**, *303*, 393–400. [\[CrossRef\]](#)
11. Huang, H.; Li, M.; Wang, L.; Liu, X.; Shen, D.; Tang, D. Gold Nanorods as Single and Combined Saturable Absorbers for a High-Energy Q-Switching Nd:YAG Solid-State Laser. *IEEE Photonics J.* **2015**, *7*, 1–10.
12. Han, M.; Zhang, S.; Li, X.; Zhang, H.; Wen, F.; Yang, Z. High-Energy, Tunable-Wavelengths, Q-Switching Pulse Laser. *Opt. Commun.* **2014**, *326*, 24–28. [\[CrossRef\]](#)
13. Keller, U.J. Recent Developments in Compact Ultrafast Lasers. *Nature* **2003**, *424*, 831–838. [\[CrossRef\]](#)
14. Zhang, Y.; Lu, D.; Yu, H.; Zhang, H.J. Low-Dimensional Saturable Absorbers in the Visible Spectral Region. *Adv. Opt. Mater.* **2019**, *7*, 1800886. [\[CrossRef\]](#)
15. Gehring, G.A.; Gehring, K.A. Co-Operative Jahn-Teller Effects. *Rep. Prog. Phys.* **1975**, *38*, 1–89. [\[CrossRef\]](#)
16. Haumesser, P.-H.; Gaumé, R.; Viana, B.; Antic-Fidancev, E.; Vivien, D. Spectroscopic and Crystal-Field Analysis of New Yb-Doped Laser Materials. *J. Phys. Condens. Matter* **2001**, *13*, 5427–5447. [\[CrossRef\]](#)
17. Liu, W.; Lu, D.; Guo, R.; Wu, K.; Pan, S.; Hang, Y.; Sun, D.; Yu, H.; Zhang, H.; Wang, J. Broadening of the Fluorescence Spectra of Sesquioxide Crystals for Ultrafast Lasers. *Cryst. Growth Des.* **2020**, *20*, 4678–4685. [\[CrossRef\]](#)
18. Kalisky, Y.; Kalisky, O.; Rachum, U.; Boulon, G.; Brenier, A. Comparative Performance of Passive Q-Switching Diode-Pumped Yb³⁺-Doped Tungstate and Garnet Lasers Using Cr⁴⁺:YAG Saturable Absorber. *IEEE J. Sel. Top. Quantum Electron.* **2007**, *13*, 502–510. [\[CrossRef\]](#)
19. Liu, J.; Tian, X.; Wu, K.; Dai, Q.; Han, W.; Zhang, H. Highly Efficient Q-Switching Laser Operation of Yb:Y₃Ga₅O₁₂ garnet crystal. *Opt. Express* **2013**, *21*, 2624–2631. [\[CrossRef\]](#)
20. Han, W.; Yi, H.; Dai, Q.; Wu, K.; Zhang, H.; Xia, L.; Liu, J. Passive Q-Switching Laser Performance of Yb:Gd₃Ga₅O₁₂ garnet crystal. *Appl. Opt.* **2013**, *52*, 4329–4333. [\[CrossRef\]](#)
21. Han, W.; Chen, X.; Xia, L.; Wang, S.; Zhang, H.; Liu, J. Continuous-Wave and Passive Q-Switching Laser Performance of Yb:YSGG Crystal. *Opt. Express* **2014**, *22*, 31404–31410. [\[CrossRef\]](#)
22. Han, W.; Chen, X.; Xia, L.; Wu, K.; Zhang, H.; Wang, S.; Liu, J.J. Efficient Passive Q-Switching Miniature Yb:Lu₃Ga₅O₁₂ Crystal Laser. *Opt. Commun.* **2015**, *349*, 15–18. [\[CrossRef\]](#)

23. Kuleshov, N.; Lagatsky, A.; Podlipensky, A.; Mikhailov, V.; Huber, G. Pulsed Laser Operation of Yb-Doped KY(WO₄)₂ and KGd(WO₄)₂. *Opt. Lett.* **1997**, *22*, 1317–1319. [[CrossRef](#)]
24. Körner, J.; Krüger, M.; Reiter, J.; Münzer, A.; Hein, J.; Kaluza, M. Temperature dependent spectroscopic study of Yb³⁺-doped KG(WO₄)₂, KY(WO₄)₂, YAlO₃ and YLiF₄ for laser applications. *Opt. Mater. Express* **2020**, *10*, 2425–2438. [[CrossRef](#)]
25. Liu, J.; Zhang, H.; Wang, J.; Petrov, V.J. Continuous-Wave and Q-Switching Laser Operation of Yb:NaY(WO₄)₂ crystal. *Opt. Express* **2007**, *15*, 12900–12904. [[CrossRef](#)] [[PubMed](#)]
26. Liu, J.; Petrov, V.; Zhang, H.; Wang, J.; Jiang, M.J. Efficient Passive Q-Switching Laser Operation of Yb in the Disordered NaGd(WO₄)₂ crystal host. *Opt. Lett.* **2007**, *32*, 1728–1730. [[CrossRef](#)]
27. Liu, J.; Petrov, V.; Zhang, H.; Wang, J. Power Scaling of a Continuous-Wave and Passive Q-Switching Yb:KLu(WO₄)₂ laser end-pumped by a high-power diode. *Appl. Phys. B* **2007**, *88*, 527–530. [[CrossRef](#)]
28. Liu, J.; Dai, Q.; Wan, Y.; Han, W.; Tian, X. The Potential of Yb:YCa₄O(BO₃)₃ crystal in generating high-energy laser pulses. *Opt. Express* **2013**, *21*, 9365–9376. [[CrossRef](#)]
29. Liu, J.; Chen, X.; Han, W.; Xu, H.; Yu, H.; Zhang, H. Passive Q-Switching Yb:YCa₄O(BO₃)₃/GaAs Laser Generating 1 mJ of Pulse Energy. *IEEE Photonics Technol. Lett.* **2016**, *28*, 1104–1106. [[CrossRef](#)]
30. Dong, L.; Liu, F.; Chen, J.; Liu, J. Research of Yb-Doped Rare-Earth Calcium Oxyborate Crystal Lasers. *Opt. Express* **2021**, *29*, 1838–1850. [[CrossRef](#)] [[PubMed](#)]
31. Chen, X.; Wang, L.; Han, W.; Guo, Y.; Xu, H.; Yu, H.; Zhang, H.; Liu, J. High-Energy Passive Q-Switching Operation of Yb:GdCa₄O(BO₃)₃ laser with a GaAs semiconductor saturable absorber. *Opt. Express* **2015**, *23*, 30357–30363. [[CrossRef](#)] [[PubMed](#)]
32. DeLoach, L.D.; Payne, S.A.; Chase, L.L.; Smith, L.K.; Kway, W.L.; Krupke, W.F. Evaluation of Absorption and Emission Properties of Yb³⁺ Doped Crystals for Laser Applications. *IEEE J. Quantum Electron.* **1993**, *29*, 1179–1191. [[CrossRef](#)]
33. Lu, D.; Pan, Z.; Zhang, R.; Xu, T.; Yang, R.; Yang, B.; Liu, Z.; Yu, H.; Zhang, H.; Wang, J. Passive Q-Switching Ytterbium-Doped ScBO₃ laser With Black Phosphorus Saturable Absorber. *Opt. Eng.* **2016**, *55*, 081312. [[CrossRef](#)]
34. Lu, D.; Pan, Z.; Yu, H.; Zhang, H.; Wang, J. Exploration of Yb³⁺: ScBO₃—A Novel Laser Crystal in the Rare-Earth Ion Doped Orthoborate System. *Opt. Mater. Express* **2015**, *5*, 1822–1833. [[CrossRef](#)]
35. Shannon, R.D. Revised Effective Ionic Radii and Systematic Studies of Interatomic Distances in Halides and Chalcogenides. *Acta Cryst. A* **1976**, *32*, 751–767. [[CrossRef](#)]
36. Zhang, H.; Meng, X.; Zhu, L.; Wang, P.; Liu, X.; Yang, Z.; Dawes, J.; Dekker, P. Growth, Morphology and Characterization of Yb:YVO₄ Crystal. *Phys. Status Solidi A* **1999**, *175*, 705–710. [[CrossRef](#)]
37. Chai, B.; Long, M.; Morris, R.; Lai, S. Crystal Growth of ScBO₃:Cr³⁺—A New Near-IR Tunable Laser Crystal. In *Tunable Solid-State Lasers II*; Springer: Berlin/Heidelberg, Germany, 1986; pp. 76–81.
38. Fang, Q.; Lu, D.; Yu, H.; Zhang, H.; Wang, J. Anisotropic Thermal Properties of Yb:YCOB Crystal Influenced by Doping Concentrations. *Opt. Mater. Express* **2019**, *9*, 1501–1512. [[CrossRef](#)]
39. Zhang, H.; Meng, X.; Zhu, L.; Liu, X.; Cheng, R.; Yang, Z.; Zhang, S.; Sun, L. Growth and Thermal Properties of Yb:Ca₄YO(BO₃)₃ Crystal. *Mater. Lett.* **2000**, *43*, 15–18. [[CrossRef](#)]
40. Nye, J.F.; Lindsay, R.B. Physical Properties of Crystals: Their Representation by Tensors and Matrices. *Phys. Today* **1957**, *10*, 26. [[CrossRef](#)]
41. Ikesue, A.; Kinoshita, T.; Kamata, K.; Yoshida, K. Fabrication and Optical Properties of High-Performance Polycrystalline Nd:YAG Ceramics for Solid-State Lasers. *J. Am. Ceram. Soc.* **1995**, *78*, 1033–1040. [[CrossRef](#)]
42. Chai, B.; Loutts, G.; Lefaucheur, J.; Zhang, X.; Hong, P.; Bass, M.; Shcherbakov, I.; Zagumennyi, A. Comparison of Laser Performance of Nd-Doped YVO₄, GdVO₄, Ca₅(PO₄)₃F, Sr₅(PO₄)₃F and Sr₅(VO₄)₃F. *OSA Proc. Adv. Solid State Lasers* **1994**, *20*, NL10.
43. Krupke, W.F. Ytterbium Solid-State Lasers. The First Decade. *IEEE J. Sel. Top. Quantum Electron.* **2000**, *6*, 1287–1296. [[CrossRef](#)]
44. Wu, K.; Hao, L.; Zhang, H.; Yu, H.; Wang, Y.; Wang, J.; Tian, X.; Zhou, Z.; Liu, J.; Boughton, R.I. Lu₃Ga₅O₁₂ Crystal: Exploration of New Laser Host Material for the Ytterbium Ion. *J. Opt. Soc. Am. B* **2012**, *29*, 2320–2328. [[CrossRef](#)]
45. Chénais, S.; Druon, F.; Balembois, F.; Lucas-Leclin, G.; Georges, P.; Brun, A.; Zavelani-Rossi, M.; Augé, F.; Chambaret, J.P.; Aka, G.; et al. Multiwatt, Tunable, Diode-Pumped CW Yb:GdCOB Laser. *Appl. Phys. B* **2001**, *72*, 389–393. [[CrossRef](#)]
46. Brenier, A.; Guyot, Y.; Canibano, H.; Boulon, G.; Ródenas, A.; Jaque, D.; Eganyan, A.; Petrosyan, A.G. Growth, Spectroscopic, and Laser Properties of Yb³⁺-Doped Lu₃Al₅O₁₂ Garnet Crystal. *J. Opt. Soc. Am. B* **2006**, *23*, 676–683. [[CrossRef](#)]
47. Yu, H.; Wu, K.; Yao, B.; Zhang, H.; Wang, Z.; Wang, J.; Zhang, Y.; Wei, Z.; Zhang, Z.; Zhang, X.; et al. Growth and Characteristics of Yb-Doped Y₃Ga₅O₁₂ Laser Crystal. *IEEE J. Quantum Electron.* **2010**, *46*, 1689–1695. [[CrossRef](#)]
48. Zuker, M.; Szabo, A.G.; Bramall, L.; Krajcarski, D.T.; Selinger, B. Delta Function Convolution Method (DFCM) for Fluorescence Decay Experiments. *Rev. Sci. Instrum.* **1985**, *56*, 14–22. [[CrossRef](#)]
49. Guillot-Noël, O.; Viana, B.; Bellamy, B.; Gourier, D.; Zogo-Mboulou, G.B.; Jandl, S. Spectroscopic Evidence of Inhomogeneous Distribution of Nd³⁺ in YVO₄, YPO₄ and YAsO₄ Crystals. *Opt. Mater.* **2000**, *13*, 427–437. [[CrossRef](#)]
50. Haumesser, P.-H.; Gaumé, R.; Viana, B.; Vivien, D. Determination of Laser Parameters of Ytterbium-Doped Oxide Crystalline Materials. *J. Opt. Soc. Am. B* **2002**, *19*, 2365–2375. [[CrossRef](#)]
51. Wang, S.; Wu, K.; Wang, Y.; Yu, H.; Zhang, H.; Tian, X.; Dai, Q.; Liu, J. Spectral and Lasing Investigations of Yb:YSGG Crystal. *Opt. Express* **2013**, *21*, 16305–16310. [[CrossRef](#)] [[PubMed](#)]

52. Koechner, W.; Bass, M. *Solid-State Lasers: A Graduate Text*; Springer Science and Business Media: Berlin/Heidelberg, Germany, 2006.
53. McDevitt, N.T.; Zabinski, J.S.; Donley, M.S.; Bultman, J.E.; Raman Band, D.-I.L.-F. Observed in Deposited MoS₂ Films. *Appl. Spectrosc.* **2016**, *48*, 733–736. [[CrossRef](#)]
54. Zhang, X.; Zhao, S.; Wang, Q.; Zhang, Q.; Sun, L.; Zhang, S. Optimization of Cr/sup 4+/-doped Saturable-Absorber Q-Switching Lasers. *IEEE J. Quantum Electron.* **1997**, *33*, 2286–2294. [[CrossRef](#)]
55. Li, D.; Xu, X.; Cheng, Y.; Cheng, S.; Zhou, D.; Wu, F.; Xia, C.; Xu, J.; Zhang, J. Crystal Growth and Spectroscopic Properties of Yb:CaYAlO₄ Single Crystal. *J. Cryst. Growth* **2010**, *312*, 2117–2121. [[CrossRef](#)]
56. Li, D.; Xu, X.; Zhu, H.; Chen, X.; De Tan, W.; Zhang, J.; Tang, D.; Ma, J.; Wu, F.; Xia, C.J.J.B. Characterization of Laser Crystal Yb:CaYAlO₄. *J. Opt. Soc. Am. B* **2011**, *28*, 1650–1654. [[CrossRef](#)]
57. Kogelnik, H.; Li, T. Laser Beams and Resonators. *Appl. Opt.* **1966**, *5*, 1550–1567. [[CrossRef](#)] [[PubMed](#)]
58. Garmire, E. Resonant Optical Nonlinearities in Semiconductors. *IEEE J. Sel. Top. Quantum Electron.* **2000**, *6*, 1094–1110. [[CrossRef](#)]
59. Fan, T.Y. Quasi-Three-Level Lasers. In *Solid State Lasers. NATO ASI Series (Series B: Physics)*; Inguscio, M., Wallenstein, R., Eds.; Springer: Boston, MA, USA, 1993; Volume 317, pp. 189–203.
60. Li, Q.; Feng, B.; Zhang, Z.; Zhang, T. Direct Numerical Simulation of quasi-Three-Level Passive Q-Switching Laser. *Opt. Commun.* **2011**, *284*, 3391–3398. [[CrossRef](#)]
61. Gupta, P.K.; Singh, A.; Sharma, S.K.; Mukhopadhyay, P.K.; Bindra, K.S.; Oak, S.M. Note: Self Q-Switching Nd:YVO₄ Laser at 914 nm. *Rev. Sci. Instrum.* **2012**, *83*, 046110. [[CrossRef](#)] [[PubMed](#)]